A rheological and microstructural study of two-step yielding in mud samples from a port area

Shakeel, Ahmad; MacIver, Michael R. ; van Kan, Paul J.M.; Kirichek, Alex ; Chassagne, Claire

DOI
10.1016/j.colsurfa.2021.126827

Publication date
2021

Document Version
Final published version

Published in
Colloids and Surfaces A: Physicochemical and Engineering Aspects

Colloids and Surfaces A: Physicochemical and Engineering Aspects 624 (2021) 126827

Contents lists available at ScienceDirect

Colloids and Surfaces A: Physicochemical and Engineering Aspects

journal homepage: www.elsevier.com/locate/colsurfa

A rheological and microstructural study of two-step yielding in mud samples from a port area

Ahmad Shakeel [a,b,*], Michael R. MacIver [c], Paul J.M. van Kan [d], Alex Kirichek [a], Claire Chassagne [a]

[a] Faculty of Civil Engineering and Geosciences, Department of Hydraulic Engineering, Delft University of Technology, Stevinweg 1, 2628 CN Delft, The Netherlands
[b] Department of Chemical, Polymer & Composite Materials Engineering, University of Engineering & Technology, New Campus, Lahore, 54890, Pakistan
[c] Norman B. Keevil Institute of Mining Engineering, The University of British Columbia, 517-6350 Stores Road, Vancouver, BC V6T 1Z4, Canada
[d] Van Kan Scientific, De Haspel 28, WX Malden, 6581, The Netherlands

HIGHLIGHTS

- Mud samples with different TOC content were analysed using rheology.
- Two-step yielding was observed in mud from amplitude and stress sweep experiments.
- Rheo-optical analysis showed the formation of cylinder-like structure during shearing.
- Larger and porous flocs were observed for samples with higher TOC content.
- This study provides a useful understanding of mud flocs during shearing.

GRAPHICAL ABSTRACT

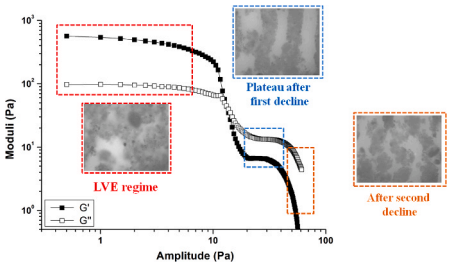

ARTICLE INFO

Keywords:
Fluid mud
Mud flocs
Rheo-optical
Fractal dimension
Moduli
Two-step yielding

ABSTRACT

Natural fine-grained suspensions usually exhibit a complex rheological fingerprint – in particular a two-step yielding phenomenon – due to the presence of mineral clay particles and organic matter (often found in a flocculated state). These rheological properties may vary considerably from one location to another due to the differences in mud composition (specifically in organic matter content). In this study, the origin of this two-step yielding behaviour for natural suspensions is discussed with the help of different experimental techniques including rheology, particle sizing, rheo-optics, and video microscopy. The samples were collected from different locations in the Port of Hamburg, Germany. A rheological analysis of the samples was performed with amplitude sweep, frequency sweep, stress ramp-up and structural recovery tests. The shear-induced structural changes of mud samples was studied by using a parallel plate shearing device with a microscope. Mineral clay-organic matter flocs were studied using video microscopy to obtain the floc size, floc density and settling velocity of flocs. Higher values of rheological properties such as cross-over stress, yield stress, and moduli were observed for samples having higher organic matter content. These samples also produced the largest floc sizes. The rheo-optical analysis showed the formation of cylinder-like structures in fine-grained suspensions upon shearing action, which reflect the origin of two-step yielding behaviour in mud samples, observed in stress ramp-up and amplitude sweep tests.

* Corresponding author at: Faculty of Civil Engineering and Geosciences, Department of Hydraulic Engineering, Delft University of Technology, Stevinweg 1, 2628 CN Delft, The Netherlands.
E-mail addresses: A.Shakeel@tudelft.nl (A. Shakeel), ryan.maciver@ubc.ca (M.R. MacIver), vankanscientific@xs4all.nl (P.J.M. van Kan), O.Kirichek@tudelft.nl (A. Kirichek), C.Chassagne@tudelft.nl (C. Chassagne).

https://doi.org/10.1016/j.colsurfa.2021.126827
Received 4 March 2021; Received in revised form 6 April 2021; Accepted 6 May 2021
Available online 12 May 2021

1. Introduction

Natural fine-grained suspensions found in harbours fall under the generic name of "mud". They typically consist of clay minerals, water, sand, silt, and a small amount of organic matter of different origin and composition [1]. A complex rheological behaviour – through a combination of yield stress, thixotropy or viscoelasticity – is usually observed in such sediments due to the combined presence of hard particles (e.g., mineral clay) and soft polymeric chains (i.e., organic matter). The rheological signature of mud is significantly dependent on the clay mineral concentration. It is reported in literature that the cohesiveness and rheological properties of mud are strongly affected by even a small amount of organic matter [2–7]. The rheological fingerprint of mud is quite important for predicting the density currents and flow of fluid mud in coastal and harbour environments. These parameters may also be used to set the boundary conditions for the modelling of sediment transport, which in turn facilitates the maintenance of dredged channels [8-11].

Several studies have been reported in the literature on the rheological analysis of cohesive mud [12-19]. For instance, a comparison of rheological properties between pure mineral clay (e.g. kaolinite) and estuarine mud samples demonstrated that the higher values of yield stress in estuarine mud samples may be attributed to the presence of organic matter [19]. Likewise, the rheological properties of kaolinite and Hendijan mud (from the Persian Gulf) were found to be strongly dependent on the water content of the mud samples [20]. Yang et al. [21] examined the rheological fingerprint of cohesive sediments obtained from three different locations in China (Yangtze River, shoal of the Hangzhou Bay and Yangcheng Lake). Those authors reported the existence of three deformation regimes in the sediment flow curves. The yield stress of mud samples is usually observed to vary exponentially as a function of the solid content of mud samples [22-25].

Recently, Shakeel et al. [24,26] examined the rheological characteristics of mud samples collected from different locations and depths of Port of Hamburg, Germany. From the extensive study, a two-step yielding phenomenon was found for the mud samples collected at the top of the water/bed interface. A similar two-step yielding for mud samples was reported by other researchers as well [23,27]. The first yield step (named "static yield"), found at very low shear rates (of the order of 0.01 s^{-1}) was attributed to the breakage of the sample structure in large flocs/clusters. The second yield step (named "fluidic yield"), observed at shear rates of the order of 10 s^{-1}, was associated with the complete destructuration of the samples. The open question remained to answer is whether the flocs/clusters formed after the static yield point had specific characteristics, linked to the sample composition and shear history. The purpose of the present article is to answer this question.

To study the influence of sample composition, video microscopy studies of settling flocs were performed to obtain the floc size and density. Many studies have investigated the size and settling velocity of mud and sand-mud flocs [28–35]. Floc size and density are dependent on their composition, their rheological (shear) history and the strength of the bonds within the floc [14,36]. In particular, in the case of clay-organic matter flocs, it has been observed that the flocs can grow larger than the Kolmogorov microscale [36]. By studying a cycle of low shear → high shear → low shear, the equilibrium floc size was found to be dependent on the shear history as well as the current applied shear. For sediments in the marine environment, floc growth and shear-dependent restructuring also depends on solid concentration (or turbidity) of the water column [37] as well as organic matter content [38].

For the present study, mud suspensions with different organic matter content were analysed. A detailed rheological analysis was conducted on the samples with amplitude sweep, frequency sweep, stress ramp-up and structural recovery tests. The shear-dependent structural changes (i.e., static and fluidic yield points) were investigated with a modified form of RheOptiCAD (i.e., a parallel plate shearing device with an upright microscope [39]), where the structural changes could be recorded by video microscopy. The main objective of the current study was to investigate the origin of two-step yielding behaviour in mud samples with the help of rheological and microstructural analysis. Therefore, the rheological results were discussed in connection to the mud floc properties (i.e., size and density) studied with settling column experiments coupled with video microscopy.

2. Experimental

The mud samples were collected from different locations of the Port of Hamburg, Germany (Fig. S1a and Table S1) using a core sampler of 1 m length. The dry density of the samples were taken to be 2650 kg m^{-3} and the bulk density was calculated by using the method reported elsewhere [14]. The particle size distribution of different mud samples, without any pre-treatment, was investigated using static light scattering (SLS) technique (Malvern MasterSizer, 2000MU) and the results are presented in Fig. S1b. The bi-modal distribution observed for P4 sample showed the presence of sand-sized particles in the mud sample. Different characteristics of the mud samples are presented in Table 1. The following sub-sections describe the rheological, rheo-optical, and floc settling velocity analyses of the collected mud samples.

2.1. Rheological analysis

A HAAKE MARS I rheometer (Thermo Scientific, Germany) with Couette geometry was used to perform the rheological characterisation of mud samples. Samples were homogenised by mild manual stirring before measurement. A constant temperature of 20 °C was maintained during each experiment with a Peltier controller system. The experiments were performed in duplicate and the repeatability error was less than 2% in all cases. To ascertain the absence of wall slip, tests were also carried out using Couette geometry with grooves on the surface and compared to the results without grooves [40]. The results were quite similar for tests with and without grooves (data not shown), which verified the absence of wall slip.

Amplitude sweep tests were performed at a constant frequency of 1 Hz to investigate the solid-to-fluid transition in the mud samples. This permitted an analysis of the linear viscoelastic (LVE) regime and cross–over stress, where the storage modulus, G', is equal to the loss modulus, G''.

Frequency sweep tests were carried out in the LVE regime using a frequency range between 0.1 and 100 Hz. The complex modulus (G^*) and phase angle (δ) were determined from storage and loss moduli and plotted as a function frequency. Stress ramp-up tests were performed by

Table 1
Characteristics of the collected mud samples.

Sample ID	Bulk density (kg m^{-3})	Water content[a] (%)	Total organic carbon (TOC) (% TS[b])	Particle size distribution percentiles from SLS		
				D_{10} (μm)	D_{50} (μm)	D_{90} (μm)
P1	1127	452	5.1	4.99 ± 0.07	23.09 ± 0.40	115.90 ± 8.39
P2	1166	337	3.7	3.94 ± 0.26	16.16 ± 0.24	81.70 ± 3.38
P3	1151	374	3.2	3.59 ± 0.03	14.71 ± 0.17	76.61 ± 3.17
P4	1305	166	2.0	4.71 ± 0.09	44.14 ± 2.41	230.36 ± 46.70

[a] Water content = based on the weight of total solid content.
[b] TS = total solids.

linearly increasing the stress (τ) at a rate of 1 Pa/s, until the shear rate ($\dot{\gamma}$) reached 300 s^{-1}. The apparent viscosity was determined from the torque and plotted against the applied shear stress. The experimental data of each stress ramp-up test was fitted with the following empirical model (Shakeel et al. [41]) to capture the two-step yielding behaviour of each mud sample:

$$\tau = \lambda\tau_{stat} + (1-\lambda)\tau_{fluid} \quad (1)$$

where the step function λ is given as

$$\lambda = 1 - \frac{1}{1+\exp(-10(\dot{\gamma}-\dot{\gamma}_0))} \quad (2)$$

The τ_{stat} term of Eq. (1) can be written as:

$$\tau_{stat} = \frac{\tau_s}{1+\dot{\gamma}_s/\dot{\gamma}} \quad (3)$$

Similarly, the τ_{fluid} term can be written as:

$$\tau_{fluid} = \tau_s + \frac{\tau_f}{1+((\dot{\gamma}_f-\dot{\gamma}_0)/(\dot{\gamma}-\dot{\gamma}_0))} + \mu_\infty(\dot{\gamma}-\dot{\gamma}_0) \quad (4)$$

In short, this empirical model contains six fitting parameters: $\dot{\gamma}_0$, τ_s, $\dot{\gamma}_s$, τ_f, $\dot{\gamma}_f$ and μ_∞.

The structural recovery test was performed according to the protocol reported in Shakeel et al. [38]. First, the geometry set position was established, then an oscillatory time sweep experiment was performed for 100 s in the LVE regime. In the second step, a steady shear rate was applied at 300 s^{-1} for 500 s. Finally, the structural recovery step was performed with the help of an oscillatory time sweep experiment within the LVE at the frequency of 1 Hz for 500 s. The pictorial representation of the experimental protocol is shown in Fig. S2. To quantify the structural recovery parameters, a stretched exponential function, adapted from [42,43], was used:

$$\frac{G'(t)}{G'_0} = \frac{G'_i}{G'_0} + \left(\left(\frac{G'_\infty - G'_i}{G'_0}\right)\left(1-\exp\left[-\left(\frac{t}{t_r}\right)^d\right]\right)\right) \quad (5)$$

where $G'(t)$ is the storage modulus of sample after breakup, G'_0 is the storage modulus before shearing (i.e. the "undisturbed" sample), G'_i is the value of storage modulus immediately after the shearing step, G'_∞ is the equilibrium storage modulus, t_r is the characteristic recovery time of the sample, d is the stretching exponent, and t is the recovery time. G'_∞, t_r, and d are the fitting parameters in Eq. (5).

2.2. Rheo-optical analysis

For the structural analysis of mud flocs under shearing action, a modified version of RheOptiCAD (detailed in Shakeel et al. [39]) was used with a 20× microscope objective. This modified RheOptiCAD has an upright microscope instead of an inverted microscope. The mud samples were diluted with tap water, to permit a clear observation of the flocs under the microscope. In all experiments, the mud flocs were deformed instead of displaced, due to the perfect contact of flocs with both upper and lower plates. The videos or images (2592 × 2048 pixels) were recorded in the x-y plane with an LED light as illumination.

Oscillatory experiments were performed using a frequency f of 1 Hz and amplitudes A between 0.1 and 0.2 mm, for the bottom plate. Continuous strain experiments were conducted by placing the mud flocs between the upper and lower plates and setting the movement of both plates in same direction at a rate of 0.003 mm/s and 0.17 mm/s for top and bottom plate, respectively. The gap between the upper and lower plate was maintained between 10 μm and 100 μm. All experiments were performed at a constant temperature of 20 °C.

2.3. Floc settling analysis

To analyse the size, shape, and settling velocity of mud flocs, video of settling experiments were performed using an apparatus similar to the one described in Ye et al. [44]. A schematic of the apparatus is shown in Fig. 1. The mud samples were diluted with tap water, drawn up with a wide-mouth pipette, then gently introduced to the water column to permit videos/images of freely settling flocs to be recorded. A custom package Safas (Sedimentation and Floc Analysis Software, [45]) was used to select flocs and determine their settling velocity from the videos. Individual flocs were then re-segmented using WEKA, a machine learning-based image segmentation tool, to obtain high quality shape and size information.

2.3.1. Mean diameter

Mean diameter, d_m [μm], was calculated from the diameter of major axis (d_{major}) and minor axis (d_{minor}) of the object in an image according to Ye et al. [44]:

$$d_m = \sqrt{d_{major} \times d_{minor}} \quad (6)$$

2.3.2. Fractal dimension

In a 2-dimensional image, the fractal dimension of an object may be related to the object's area and perimeter according to Meakin [46]:

$$P \propto A^{1/2}$$

where P [μm] and A [μm^2] are the perimeter and area of the object in the binary image. A log-log plot of perimeter versus area was used to calculate the perimeter-based fractal dimension, D_p. Values for D_p may vary between: 1, for a massive structure; and 2, for a completely filamentous or extended structure [47].

2.3.3. Effective density of mud flocs

The effective density of a floc, ρ_e, is:

$$\rho_e = \rho_f - \rho_w \quad (7)$$

where ρ_e, ρ_f, and ρ_w are the floc, solid, and water density, respectively. For an estimate of floc effective density, Stokes' Law was used to plot isolines 10, 100, and 1000 kg m^{-3} with:

$$v = \frac{2}{9}\frac{\rho_e}{\mu}g\left(\frac{d_m}{2}\right)^2 \quad (8)$$

where v is the floc settling velocity, μ is the viscosity of water, g is the acceleration due to gravity and d_m is the mean diameter of the floc.

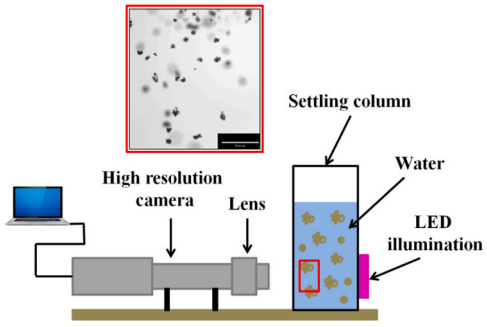

Fig. 1. Schematics of the settling column apparatus used for the floc analysis.

3. Results and discussion

3.1. Rheological analysis of mud

3.1.1. Amplitude sweep tests

Oscillatory amplitude sweep tests were carried out to investigate the solid-liquid transition in mud samples, when a cross-over between storage, G', and loss, G'', moduli occurs. A suitable frequency was chosen for amplitude sweep tests by performing preliminary tests at different frequencies (data not presented). Those results showed that the higher frequencies were not suitable for amplitude sweep tests because the cross-over between G' and G'' was absent. Therefore, a frequency of 1 Hz was selected to perform all remaining amplitude sweep tests.

The storage and loss moduli are plotted as a function of amplitude for different mud samples in Fig. 2a. A two-step yielding behaviour is evident from Fig. 2a for all investigated samples. In Fig. 2a, the first yield (i.e. static) occurred at different values for each sample between 5 and 12 Pa; while the second yield for each sample occurred between 25 and 41 Pa. Furthermore, two important characteristics may be identified from Fig. 2a: (i) a linear viscoelastic regime where moduli are more or less independent of amplitude, which may be considered a solid-like impression and (ii) a solid-to-fluid transition where the moduli G' and G'' cross each other. This information about solid-liquid transition in mud samples can be quite important where the destruction of mud/floc structure is required (e.g., for navigational purposes). The stress corresponding to this transition state, when $G' = G''$, is referred to as the cross-over stress and is presented in Fig. 2b for different samples. It is shown that the cross-over stress of samples P1 and P2, with a higher organic matter content, occurred at higher values than samples with lower organic matter content, which is consistent with the results already reported in the literature for mud [24].

3.1.2. Frequency sweep tests

Frequency sweep tests were performed at an oscillatory amplitude within the LVE regime, where the structure was undisturbed, with a frequency from 0.1 to 100 Hz. These experiments are suitable to investigate the mechanical behaviour (i.e., strength) and microstructure of mud samples without affecting their structure. In Fig. S3a and b, the results of frequency sweep tests are presented in terms of complex modulus and phase angle as a function of applied frequency for different samples. A solid-like behaviour of the mud samples was found from the weak frequency dependency of the complex modulus and the smaller phase angle values. Similar results of the solid-like character of mud samples have been reported in the literature [20,19,25]. The experimental data at higher frequencies was unreliable due to rheometer head inertial effects and, therefore, not included in the analysis.

To compare the characteristics of different mud samples, complex modulus and phase angle at 1 Hz are plotted in Fig. 3a and b, respectively. In Fig. 3a, samples P1 and P2 showed higher moduli values compared to the other two samples, which may be linked, as in the case of the cross-over stress, to the presence of higher organic matter content. However, sample P2 is an anomaly, with an even higher modulus than P1 sample. Although the amount of organic matter is lower in P2 sample, it has a slightly higher density (Table 1). It has already been shown that the modulus is strongly correlated with density of mud [48]. The values of phase angle (i.e., degree of structuration [49]) were more or less constant for the samples investigated (Fig. 3b), which indicated that this parameter was not particularly sensitive to the organic matter content or mass density of the samples.

3.1.3. Stress ramp-up tests

The yield stress of mud samples was determined from stress ramp-up tests because they are considered as a reliable yield stress analysis. The outcome of this test is shown in Fig. S4, with apparent viscosity plotted as a function of stress for different mud samples. This experiment also verified the existence of two-step yielding behaviour observed in the amplitude sweep tests, which is discussed in more detail in Section 3.2. To explain the two-step yielding behaviour observed in mud samples, an empirical model (Eq. (1)) was used to fit the experimental data of stress ramp-up tests. The values of the fitting parameters are presented in Table S2 for different mud samples. Two important parameters, τ_s and τ_f which represent the static and fluidic yield stresses (i.e., two yield points) of samples are plotted in Fig. 4a and b, respectively. This test confirmed the higher yield stresses of samples P1 and P2 compared to samples P3 and P4, which may be attributed to the higher organic matter content of samples P1 and P2.

3.1.4. Structural recovery tests

The structural recovery of mud samples after breakup was investigated with a three step protocol [38]. In the final step, the storage modulus was recorded as a function of time, within the LVE regime, to quantify the structural recovery of mud. The structural growth after pre-shearing for different mud samples, is shown in Fig. S5, in terms of normalised storage modulus, G'/G'_0, as a function of time. An empirical model (Eq. (5)) was further used to obtain the structural recovery parameters by fitting the experimental data. The values of the model parameters are shown in Table S3. The extent of recovery (G'_∞/G'_0) and the characteristic time of recovery, (t_r), are plotted in Fig. 5a and b, respectively for different mud samples.

Sample P4 exhibited the highest structural recovery while sample P1 showed the lowest, which may be associated with the different

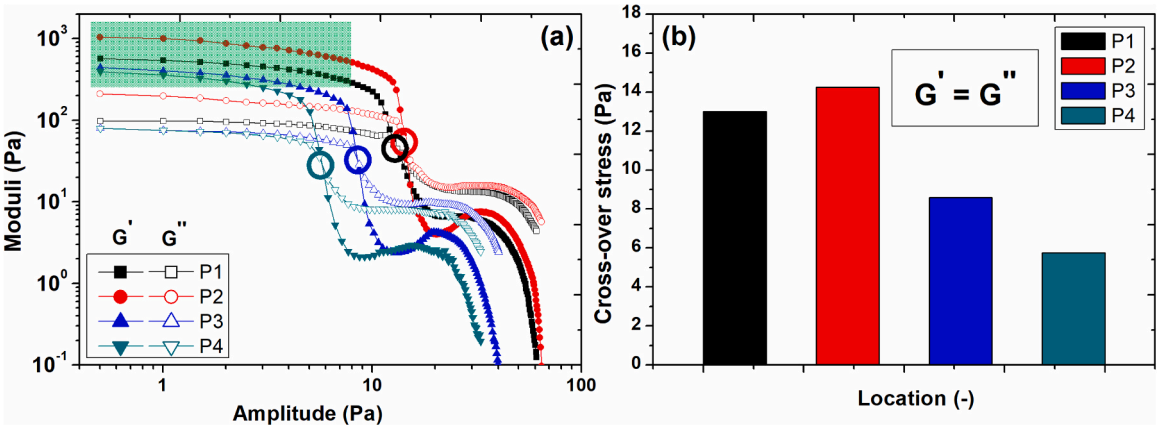

Fig. 2. (a) Storage (filled symbols), G' and loss (empty symbols), G'' moduli as a function of oscillation amplitude for different mud samples at 1 Hz. The shaded region represents the LVE regime and the circles represent the cross-over between G' and G'', (b) cross-over stress values (i.e., when $G' = G''$) for different mud samples obtained from amplitude sweep tests.

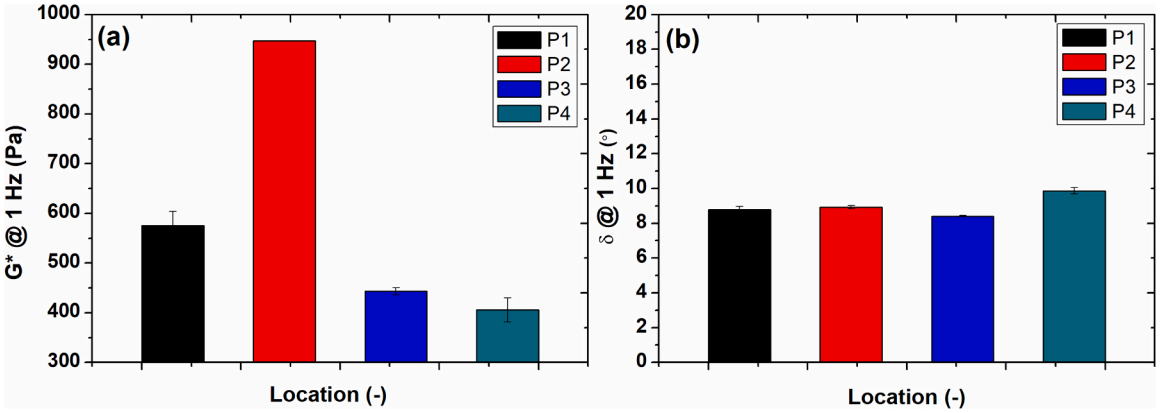

Fig. 3. (a) Complex modulus (G^*) and (b) phase angle (δ) at 1 Hz for different mud samples. Bars represent standard deviation.

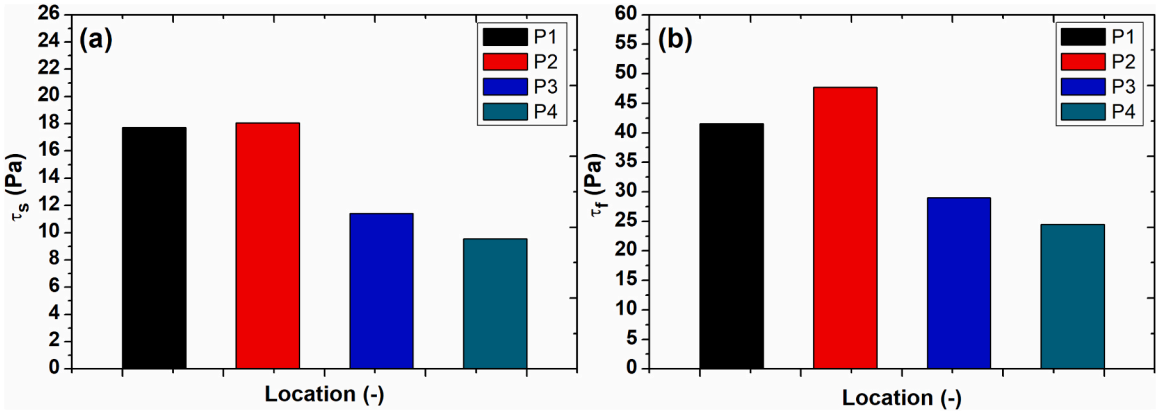

Fig. 4. (a) Static (τ_s) and (b) fluidic (τ_f) yield stresses obtained from the fitting of Eq. (1) for different mud samples.

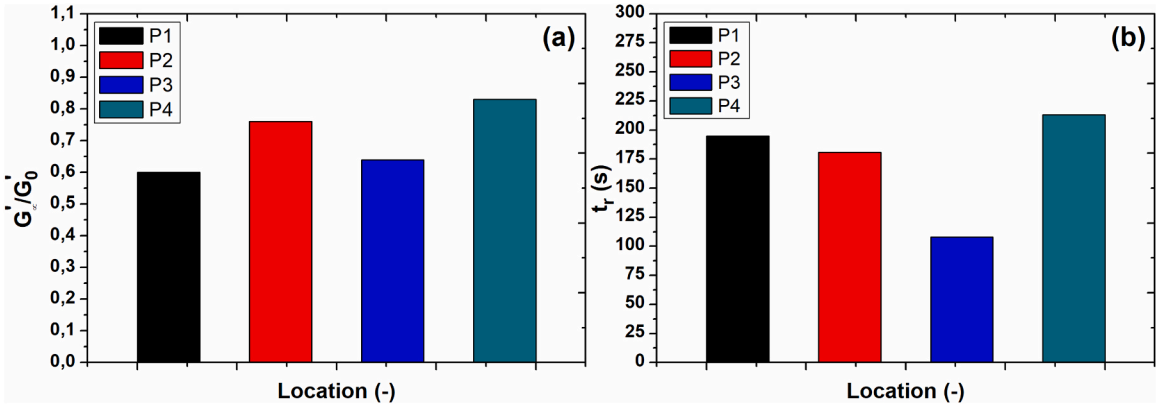

Fig. 5. (a) Equilibrium structural recovery (G'_∞/G'_0) and (b) characteristic recovery time (t_r) obtained from the fitting of Eq. (5) for different mud samples.

organic matter content in these samples [38]. Furthermore, the enhanced recovery in sample P4 may be due the higher silt/sand content in that sample, which is also observable in the bi-modal distribution of the PSD of that sample in Fig. S1b. The silt/sand fraction of a sample will tend to settle during shearing, which leads to a clay dominant, structured system, that may achieve a higher structural recovery [14]. The settling of silt/sand particles during shear flow of sand-clay mixtures and the consequential enhancement in the rheological properties has also been reported in literature [50]. On the other hand, the extensive pre-shearing of mud samples with highest organic matter content (such as sample P1) may result in severe re-organisation and deterioration of polymeric chains [38], which could contribute to a reduced extent of recovery, (G'_∞/G'_0), as shown in Table S3.

All samples, except P3, showed quite a high characteristic time of recovery (t_r) (Fig. 5b), which means a stronger and slower recovery for samples P2 and P4 and a weaker and slower recovery for P1 sample. The behaviour of sample P3 was quite interesting, particularly in terms of characteristic time. This sample showed slightly higher structural recovery than P1 sample, although the amount of organic matter is significantly lower than P1 sample. Furthermore, the smallest characteristic time was observed for P3 sample, which depicts stronger recovery than sample P1 with a shorter recovery time. This observation

cannot be fully explained in terms of organic matter and solids concentration. Our preliminary analysis as a function of ionic composition (obtained during the same campaign, see Table S4) indicates that the type and concentration of ions may contribute to differences in structural recovery, but this requires further systematic investigation.

3.2. Rheo-optical analysis of mud

In the literature, the two-step yielding phenomenon has been observed in diverse systems, including carbopol microgel [51], colloidal glasses [52], capillary suspensions [53], silica dispersions [54], surfactant pastes [55], magneto-rheological systems [56], muscovite dispersions [57] and mud suspensions [24]. Typically, this two-step yielding has been explained by the breakage of inter-connected network of flocs/clusters (i.e., first yield, named "static yield" in the present article) followed by the disruption of individual flocs/clusters (i.e., second yield or "fluidic yield") [26,58]. A more in-depth study of the structure of the samples was performed by rheo-optical analysis after first and second yield points were measured.

The RheOptiCAD oscillatory shearing test was performed by placing the diluted mud sample between two plates, at a frequency of 1 Hz. The extracted images from the recorded video are shown in Fig. 6 for P1 sample. At the onset of shearing (Fig. 6a), an inter-connected network of mud flocs was observed, which is mainly responsible for the higher moduli values within LVE (Fig. 2a), for complex moduli and phase angle values at 1 Hz in frequency sweep tests (Fig. 3) and for higher apparent viscosity values before first decline in stress ramp-up tests (Fig. S4). After further shearing, this floc network started to collapse, which represents the first (static) yield point in the amplitude sweep and stress ramp-up tests. After breakage of the inter-connected floc network, continued shearing resulted in the formation of hollow cylinder-like structures (Fig. 6b and c), which resisted the application of shear. Therefore, the plateau behaviour after the first decline in amplitude sweep and stress ramp-up tests (in between the first and second yield step) was attributed to these cylinder-like structures. These structures were also observed in samples (P2–P4) (Fig. 7), although the samples from P4 were irregularly shaped, likely due to the presence of larger silt/sand particles, which may have hindered the re-orientation of organic matter to create the structures observed in other samples.

The formation of similar cylinder-like structures (referred to as log-rolling flocs in Varga et al. [59]), by shearing between parallel plates or in a Couette cell, has been reported in literature for different weakly attractive suspensions (e.g., carbon black particles in mineral oil, polyamide particles in water or water/glycerine mixture and hollow glass spheres in mineral oil) [59]. In Fig. S6, the structures from our study are presented with those from Varga et al. [59]. Varga et al. [59] attributed the formation of these structures to the hydrodynamic coupling between the confining geometry and flocs, which was verified by experiments and simulations. Furthermore, the authors have also studied the influence of strain on the formation of log-rolling flocs and the influence of the gap between the plates on the stability of the flocs, as a function of the ratio between gap size and mean particle radius. Likewise, the development of log-rolling structures as a function of shearing action along with the existence of two-step yielding at higher solid content, in oscillatory amplitude sweep tests, has been reported in literature for silica rod suspensions [60].

These cylinder-like structures break down into smaller flocs on continuous shearing (Fig. 6d), which is associated with the second yield point observed in the rheological tests. Therefore, the possible mechanism of two-step yielding reported previously for mud suspensions [26, 38], – i.e. the breakage of inter-connected network of flocs (static yield) followed by the collapse of individual flocs into particles or smaller flocs (fluidic yield) – was verified by this structural analysis. The true explanation about the existence of a plateau after the first decline was missing from that prior analysis, but has been elucidated here with a description of the cylinder-like structure formation that occurs in the samples. The complete mechanism of two-step yielding is pictorially presented in Fig. 8.

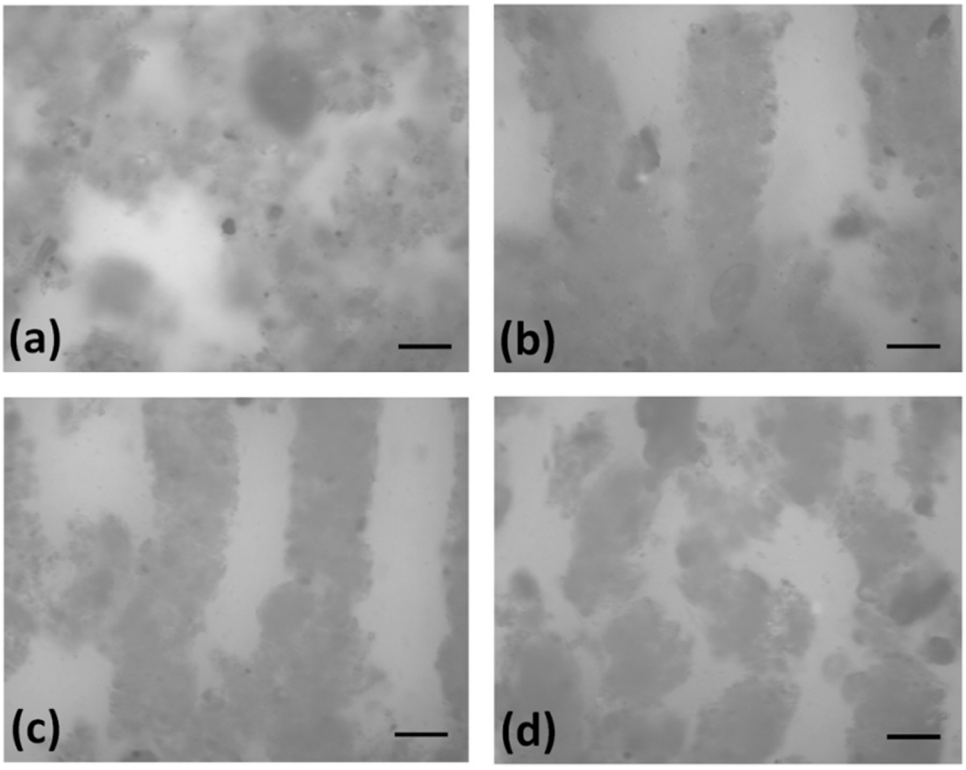

Fig. 6. The snapshots from the recorded video at (a) t = 2 s, (b) t = 30 s, (c) t = 50 s and (d) t = 100 s for P1 sample oscillatory sheared at a frequency of 1 Hz and amplitude of 0.1 mm with the gap between the plates of 20 μm. The scale bar represents 70 μm.

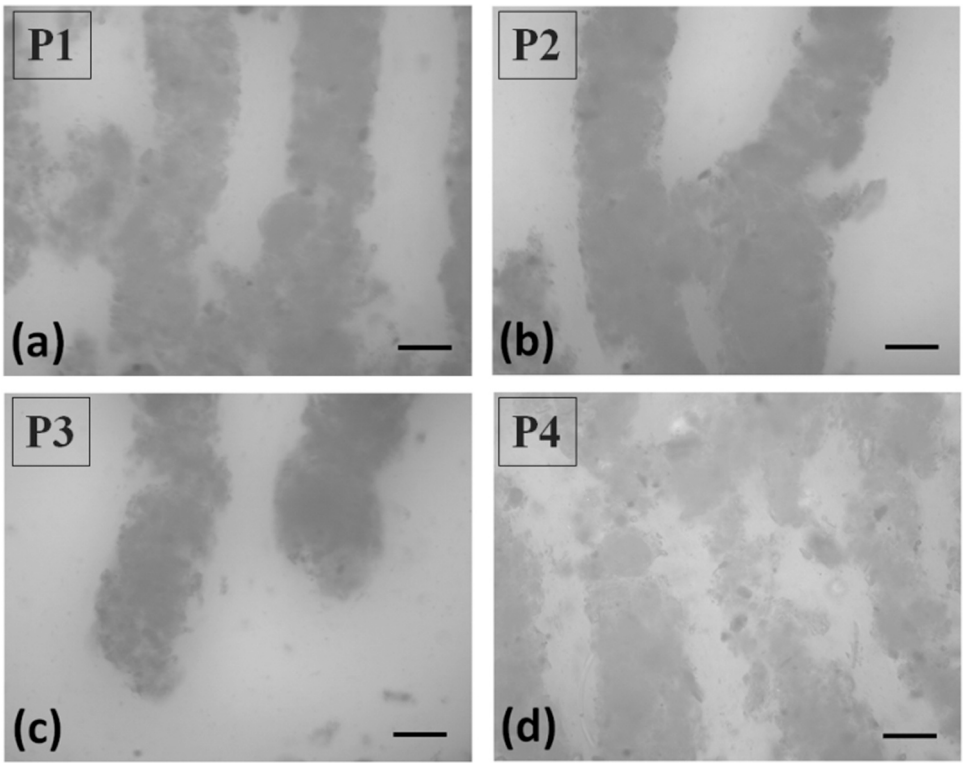

Fig. 7. The snapshots from the recorded video at t = 50 s for (a) P1 sample, (b) P2 sample, (c) P3 sample and (d) P4 sample oscillatory sheared at a frequency of 1 Hz and amplitude of 0.1–0.2 mm with the gap between the plates of 10–100 μm. The scale bar represents 70 μm.

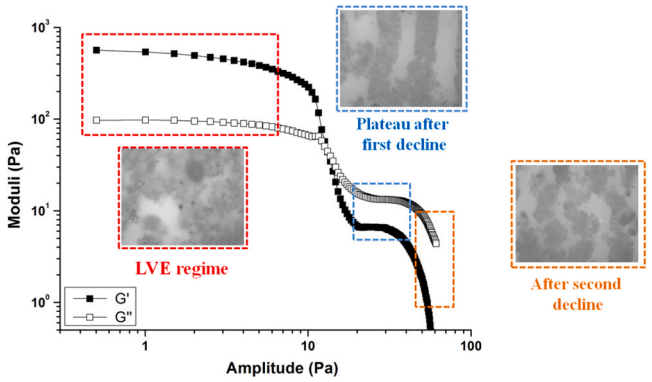

Fig. 8. Schematics of the two-step yielding observed by amplitude sweep tests for mud samples.

These cylinder-like structures were also exposed to the continuous strain experiments by setting the movement of both plates in same direction but at different rates. Selected images from the video are shown in Fig. S7. It was found that the cylinder-like structure followed the movement/rolling in the direction of faster moving plate without any breakage. However, in stress ramp-up tests, a second decline in viscosity was observed, which suggests the destruction of these cylinder-like structures. The absence of breakage of these cylinder-like structures in rheo-optical experiments may be attributed not only to the significantly lower shear rate of the parallel plate measurement (compared with the higher shear of the rheological experiments) but also due to the sample dilution required for this analysis (i.e. no neighbouring effect).

3.3. Settling analysis of mud flocs

In the last part, the particle (floc) shape and density was investigated prior to shearing to determine whether a correlation could be found between floc properties and the rheological properties and cylinder-like structures observed in rheological and rheo-optical experiments. To analyse the mud floc size, settling velocity and to derive their density, settling experiments were performed with the experimental setup presented in Fig. 1. A few flocs from a single video frame of P2 location are shown in Fig. 9.

In Fig. 10, floc settling velocity is plotted against floc size (mean diameter) for mud samples obtained from different locations. A similar correlation between the settling velocity and the size of flocs has also been observed in literature [61-64]. Effective floc density was calculated with Stokes Law according to Eq. (8). These results show that the spread in effective density is aligned with the trend in the organic matter content (TOC), i.e., P1 > P2 > P3 > P4 (Table 1). The sample from

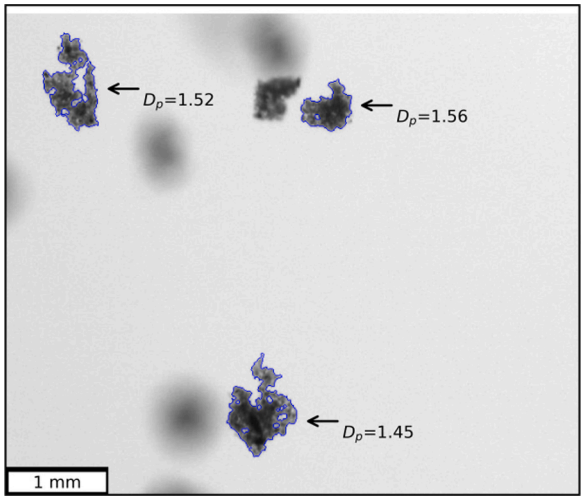

Fig. 9. Flocs from a single video frame of P2 sample along with the values of perimeter-based fractal dimension (D_p).

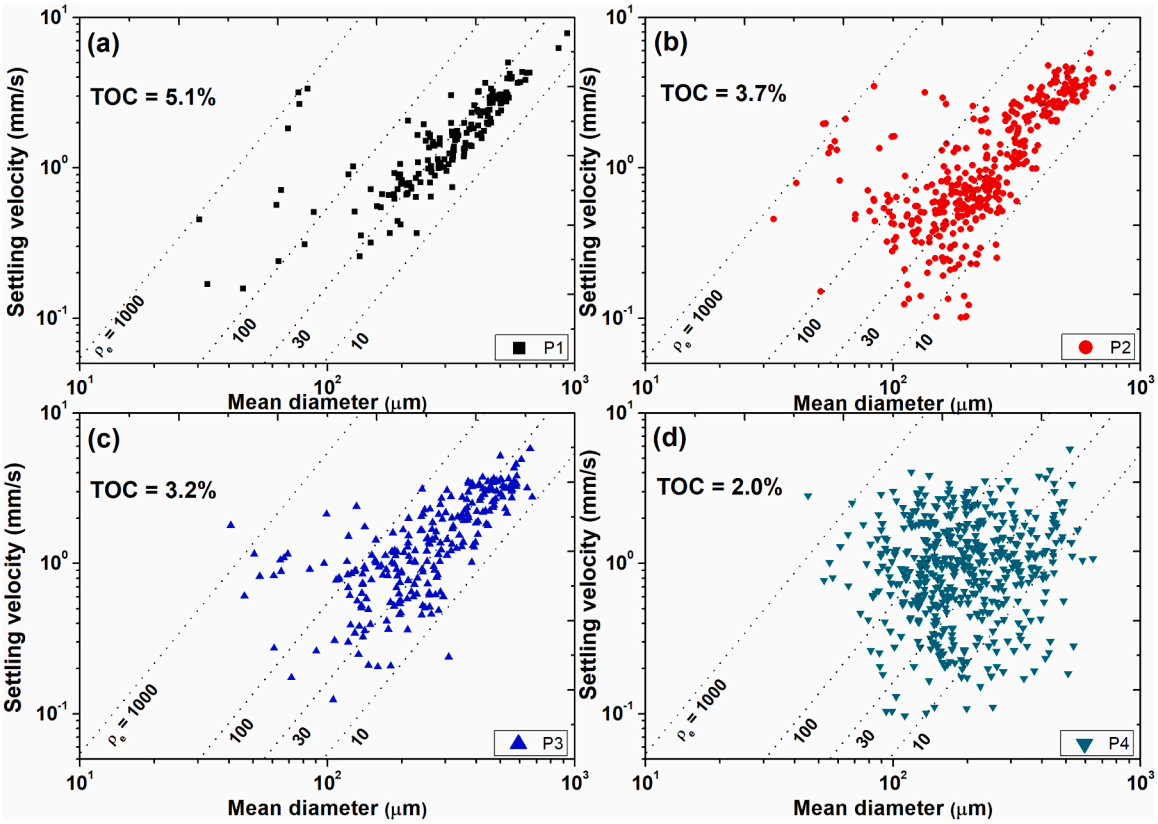

Fig. 10. Settling velocity as a function of mean diameter for mud flocs from (a) location P1, (b) location P2, (c) location P3 and (d) location P4. Dashed lines represent the iso-lines derived from Eq. (8).

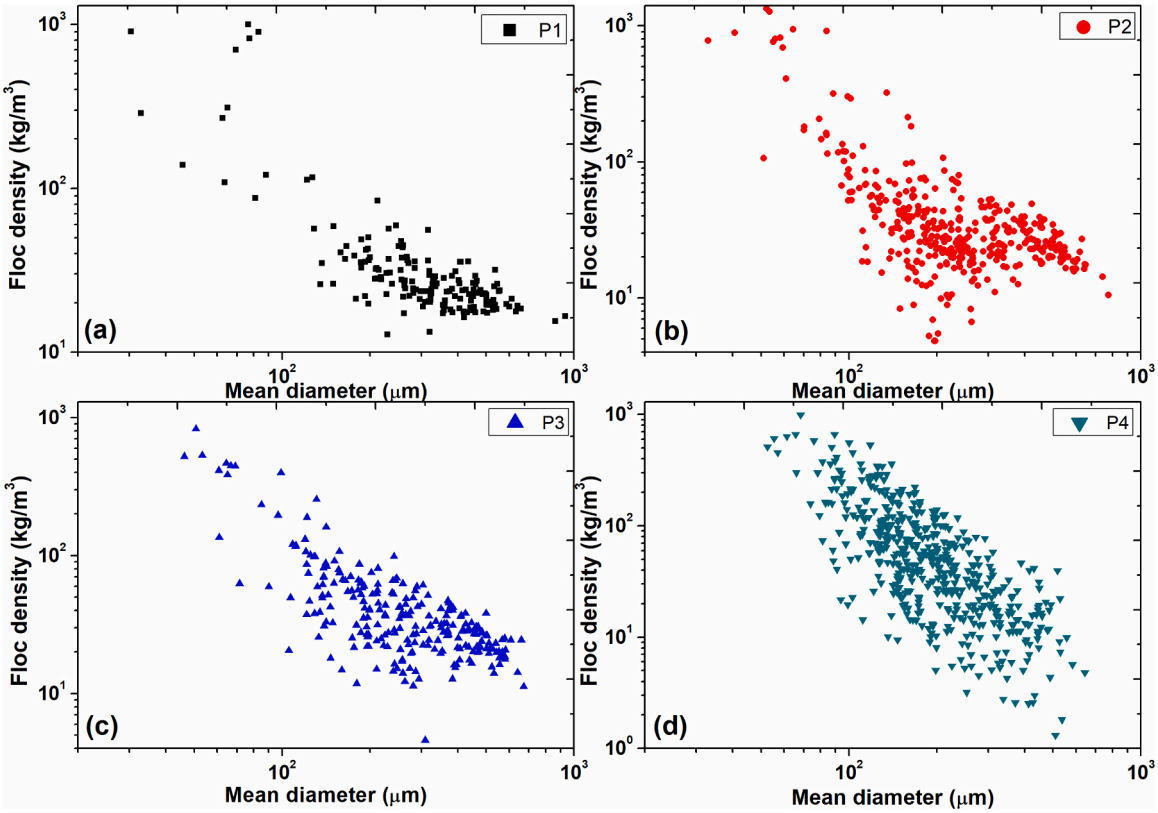

Fig. 11. Effective floc density as a function of mean diameter for mud flocs from (a) location P1, (b) location P2, (c) location P3 and (d) location P4.

location P1 displayed a relatively consistent effective density and a linear relationship between log(settling velocity) and log(floc size); whereas, sample P4, with the lowest organic matter content, showed a much larger spread in effective density values. For example, in case of P1 sample, the flocs appear to fall along the 30 kg m^{-3} iso-line, while for P4 sample, there was a wide spread in excess density values from below 10 kg m^{-3} to above 800 kg m^{-3}. Based on the effective density relation, Eq. (7), this is equivalent to an effective density between 1.01 and 1.8 kg m^{-3}. In Fig. S8, the perimeter-based fractal dimension is calculated for the flocs as two times the slope of the log-log plot of perimeter versus area. This method for calculating the fractal dimension has been used in many studies [65-70], therefore, it provides a convenient means of comparing the structural characteristics of flocs between different studies. From the plot of perimeter-based fractal dimension, it was found that P4 sample has the smallest value of D_p, which is an indication of tightly packed, less open, or less porous mud flocs – having, hence, a larger density. The mud samples from other locations (P1, P2 and P3) displayed similar values of D_p, within the range of 1.32–1.34.

The correlation between the settling velocity and the aspect ratio of the flocs for different locations is shown in Fig. S9. The result shows that the flocs with higher aspect ratio displayed lower settling velocity, for locations P1 and P2. For P3 and P4, there is no trend between aspect ratio and settling velocity. This result is in line with the TOC of these samples: larger amounts of organic matter tend to produce organic matter-rich flocs, which are highly cohesive and lead to the formation of elongated flocs by macro-aggregation of two flocs.

The effective density of flocs is presented as a function of size of flocs in Fig. 11, which shows an exponential decay in floc density on a log-log plot, as is usually found in literature [71-75]. The similar trend can also be seen from the images of the flocs, as shown in Fig. S10. In Fig. 12, a histogram of the mean diameter is shown for each sample and the mean floc size was calculated as the simple mean of the measured values. The mean floc size was found to decrease in the following order: P1 > P3 > P2 > P4. This result also confirms that the floc size was largest for P1 sample (having highest organic matter content) and smallest for sample P4 (with lowest organic matter content). The presence of larger organic matter-rich flocs in sample P1 also justifies the higher values of rheological parameters such as cross-over stress, moduli, and yield stresses. Furthermore, the lowest amount of organic matter in P4 samples resulted in higher average effective density, smaller floc size, and higher settling rates of the flocs.

4. Conclusions

Fine-grained suspensions typically exhibit a complex rheological fingerprint due to the presence of hard clay particles and flexible chains of organic matter. The rheological properties of mud suspensions, with same density, can considerably vary from one location to another due to the differences in composition (particularly organic matter content). Therefore, in this study, mud samples from different locations of Port of Hamburg, Germany were analysed by using amplitude sweep, frequency sweep, stress ramp-up and structural recovery tests. The results showed that the samples containing higher amount of organic matter (i.e., P1 and P2) displayed higher values of rheological properties such as cross-over stress, yield stress, and moduli. However, the structural recovery after breakup (G'_{∞}/G'_0) was observed to be lowest for P1 sample, which may be attributed to the severe re-organisation/deterioration of organic matter, which were not able to recuperate their original state after removal of shear. Furthermore, the rate of structural recovery was fastest (i.e., smallest value of t_r) in case of P3 sample, which may be associated to the presence of a higher concentration of ions in this sample, which needs to be further investigated. All the mud samples displayed a two-step yielding behaviour in amplitude sweep and stress ramp-up tests.

To understand the origin of this two-step yielding behaviour, the structural organisation upon shearing of mud samples was examined

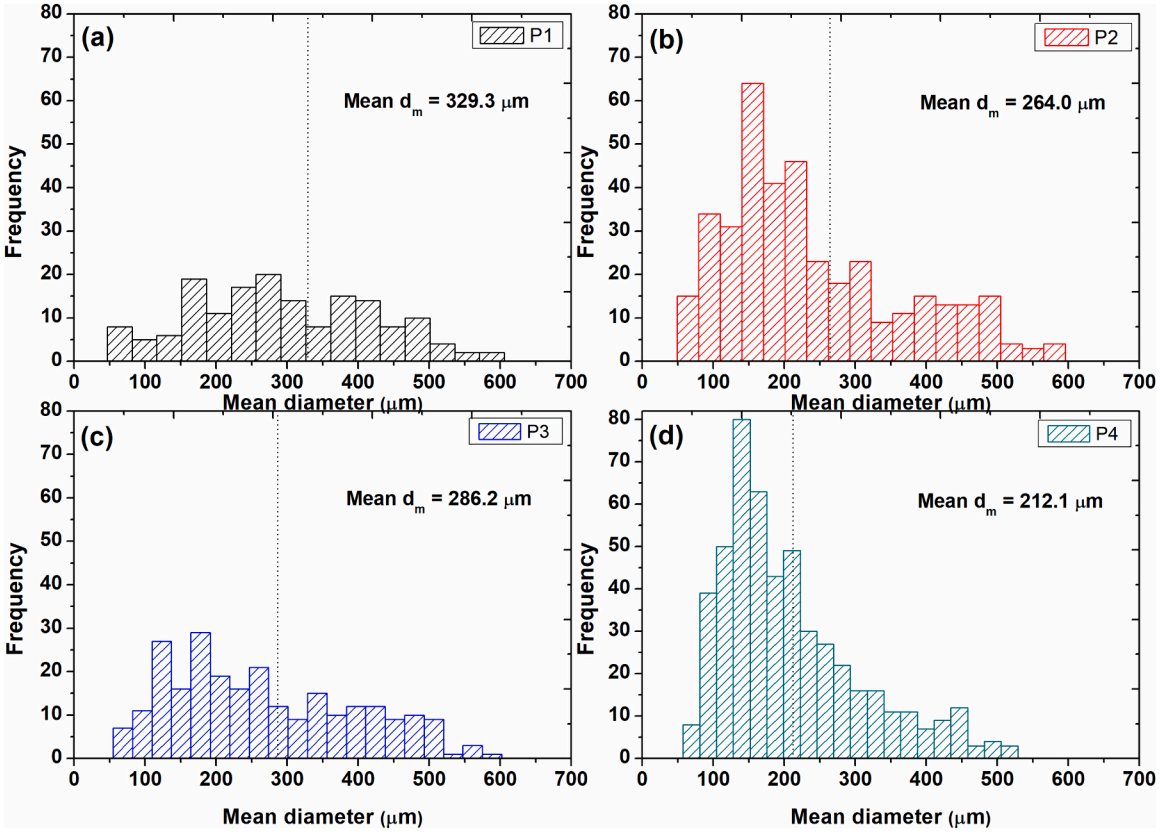

Fig. 12. Floc size distribution for mud flocs from (a) P1 location, (b) P2 location, (c) P3 location and (d) P4 location with mean value of diameter marked with a vertical dashed line and the value is shown at the top right of each plot.

by using modified form of RheOptiCAD. The RheOptiCAD analysis confirmed the formation of cylinder-like structures in mud suspensions upon shearing action, which explains the second plateau observed in stress ramp-up and amplitude sweep tests. Therefore, the first decline in viscosity or moduli (i.e. static yield) may be linked to the breakage of inter-connected network of flocs while the second decline (i.e. fluidic yield) may be associated to the breakage of cylinder-like structures formed upon further shearing. In the final part, the detailed analysis of mud flocs was performed with the help of floc-camera settling setup, to obtain the floc size, density and settling velocity. The floc analysis confirmed the formation of larger flocs with higher aspect ratio (open and porous structure) for the samples with higher organic matter content (P1 and P2 locations), which explains the higher rheological properties for these samples. For P4 location, the scattered behaviour of settling velocity as a function of floc size revealed the presence of silt/sand particles, as confirmed by PSD analysis from laser diffraction technique. The RheOptiCAD analysis of sample from P4 location showed the formation of irregular cylinder-like structures, which was similarly attributed to the presence of silt/sand. This study provides a useful understanding of correlation between the rheological signature and floc characteristics of natural fine-grained suspensions.

CRediT authorship contribution statement

Ahmad Shakeel: Methodology, Investigation, Formal analysis, Writing - original draft. **Michael R. MacIver:** Formal analysis, Software, Visualization. **Paul J.M. van Kan:** Resources, Writing - review & editing. **Alex Kirichek:** Conceptualization, Supervision, Writing - review & editing. **Claire Chassagne:** Funding acquisition, Supervision, Writing - review & editing.

Declaration of Competing Interest

The authors declare that they have no known competing financial interests or personal relationships that could have appeared to influence the work reported in this paper.

Acknowledgement

This study is funded by the Hamburg Port Authority and carried out within the framework of the MUDNET academic network: https://www.tudelft.nl/mudnet/. M.R. MacIver kindly acknowledges support from the Natural Sciences and Engineering Research Council of Canada in the form of a PGS-D scholarship and the Michael Smith Foreign Study Supplement.

Appendix A. Supplementary material

Supplementary data associated with this article can be found in the online version at doi:10.1016/j.colsurfa.2021.126827.

References

[1] J. Berlamont, M. Ockenden, E. Toorman, J. Winterwerp, The characterisation of cohesive sediment properties, Coast. Eng. 21 (1) (1993) 105–128.
[2] J. Malarkey, J.H. Baas, J.A. Hope, R.J. Aspden, D.R. Parsons, J. Peakall, D. M. Paterson, R.J. Schindler, L. Ye, I.D. Lichtman, The pervasive role of biological cohesion in bedform development, Nat. Commun. 6 (2015) 6257.
[3] D.R. Parsons, R.J. Schindler, J.A. Hope, J. Malarkey, J.H. Baas, J. Peakall, A. J. Manning, L. Ye, S. Simmons, D.M. Paterson, R.J. Aspden, S.J. Bass, A.G. Davies, I. D. Lichtman, P.D. Thorne, The role of biophysical cohesion on subaqueous bed form size, Geophys. Res. Lett. 43 (4) (2016) 1566–1573.
[4] D.M. Paterson, R.M. Crawford, C. Little, Subaerial exposure and changes in the stability of intertidal estuarine sediments, Estuar. Coast. Shelf Sci. 30 (6) (1990) 541–556.
[5] D.M. Paterson, S.E. Hagerthey, in: K. Reise (Ed.), Ecological Comparisons of Sedimentary Shores, Springer Berlin Heidelberg, Berlin, Heidelberg, 2001, pp. 105–125.
[6] R.J. Schindler, D.R. Parsons, L. Ye, J.A. Hope, J.H. Baas, J. Peakall, A.J. Manning, R.J. Aspden, J. Malarkey, S. Simmons, D.M. Paterson, I.D. Lichtman, A.G. Davies, P.D. Thorne, S.J. Bass, Sticky stuff: redefining bedform prediction in modern and ancient environments, Geology 43 (5) (2015) 399–402.
[7] A. Shakeel, A. Kirichek, C. Chassagne, Is density enough to predict the rheology of natural sediments? Geo-Mar. Lett. 39 (5) (2019) 427–434.
[8] A. Kirichek, C. Chassagne, H. Winterwerp, T. Vellinga, How navigable are fluid mud layers? Terra Aqua 151 (2018) 6–18.
[9] E.B. May. Environmental Effects of Hydraulic Dredging in Estuaries, Alabama Marine Resources Laboratory, 1973.
[10] W.R. Parker, R. Kirby, Estuarine Comparisons, Academic Press, 1982, pp. 573–589.
[11] R. Whitehouse, R. Soulsby, W. Roberts, H. Mitchener. Dynamics of Estuarine Muds: A Manual for Practical Applications, Thomas Telford, 2000.
[12] B. Babatope, P.R. Williams, D.J.A. Williams, Cohesive sediment characterization by combined sedimentation and rheological measurements, J. Hydraul. Eng. 134 (9) (2008) 1333–1336.
[13] Y.C. Bai, C.O. Ng, H.T. Shen, S.Y. Wang, Rheological properties and incipient motion of cohesive sediment in the Haihe Estuary of China, China Ocean Eng. 16 (4) (2002) 483–498.
[14] P. Coussot, Mudflow Rheology and Dynamics, CRC Press, Rotterdam, 1997.
[15] P. Coussot, Rheophysics of pastes: a review of microscopic modelling approaches, Soft Matter 3 (5) (2007) 528–540.
[16] R.W. Fass, S.I. Wartel, Rheological properties of sediment suspensions from Eckernforde and Kieler Forde Bays, Western Baltic Sea, Int. J. Sediment Res. 21 (1) (2006) 24–41.
[17] Z. Huang, H. Aode, A laboratory study of rheological properties of mudflows in Hangzhou Bay, China, Int. J. Sediment Res. 24 (4) (2009) 410–424.
[18] F. Jiang, A.J. Mehta, Mudbanks of the southwest coast of India IV: mud viscoelastic properties, J. Coast. Res. 11 (3) (1995) 918–926.
[19] T. Van Kessel, C. Blom, Rheology of cohesive sediments: comparison between a natural and an artificial mud, J. Hydraul. Res. 36 (4) (1998) 591–612.
[20] M. Soltanpour, F. Samsami, A comparative study on the rheology and wave dissipation of kaolinite and natural Hendijan Coast mud, the Persian Gulf, Ocean Dyn. 61 (2) (2011) 295–309.
[21] W. Yang, G.-l. Yu, S.k. Tan, H.-k. Wang, Rheological properties of dense natural cohesive sediments subject to shear loadings, Int. J. Sediment Res. 29 (4) (2014) 454–470.
[22] D.L. Fonseca, P.C. Marroig, J.C. Carneiro, M.N. Gallo, S.B. Vinzón, Assessing rheological properties of fluid mud samples through tuning fork data, Ocean Dyn. 69 (1) (2019) 51–57.
[23] S. Nie, Q. Jiang, L. Cui, C. Zhang, Investigation on solid-liquid transition of soft mud under steady and oscillatory shear loads, Sediment. Geol. 397 (2020), 105570.
[24] A. Shakeel, A. Kirichek, C. Chassagne, Rheological analysis of mud from Port of Hamburg, Germany, J. Soils Sediment. 20 (2020) 2553–2562.
[25] J. Xu, A. Huhe, Rheological study of mudflows at Lianyungang in China, Int. J. Sediment Res. 31 (1) (2016) 71–78.
[26] A. Shakeel, A. Kirichek, C. Chassagne, Yield stress measurements of mud sediments using different rheological methods and geometries: an evidence of two-step yielding, Mar. Geol. 427 (2020), 106247.
[27] A.J. Mehta, F. Samsami, Y.P. Khare, C. Sahin, Fluid mud properties in nautical depth estimation, J. Waterw. Port Coast. Ocean Eng. 140 (2014) 210–222.
[28] A.J. Manning, J.V. Baugh, J.R. Spearman, E.L. Pidduck, R.J.S. Whitehouse, The settling dynamics of flocculating mud-sand mixtures: part 1—empirical algorithm development, Ocean Dyn. 61 (2) (2011) 311–350.
[29] A.J. Manning, J.V. Baugh, J.R. Spearman, R.J.S. Whitehouse, Flocculation settling characteristics of mud: sand mixtures, Ocean Dyn. 60 (2) (2010) 237–253.
[30] A.J. Mehta, A.J. Manning, Y.P. Khare, A note on the Krone deposition equation and significance of floc aggregation, Mar. Geol. 354 (2014) 34–39.
[31] R.L. Soulsby, A.J. Manning, J. Spearman, R.J.S. Whitehouse, Settling velocity and mass settling flux of flocculated estuarine sediments, Mar. Geol. 339 (2013) 1–12.
[32] J.R. Spearman, A.J. Manning, R.J.S. Whitehouse, The settling dynamics of flocculating mud and sand mixtures: part 2—numerical modelling, Ocean Dyn. 61 (2) (2011) 351–370.
[33] K.L. Spencer, A.J. Manning, I.G. Droppo, G.G. Leppard, T. Benson, Dynamic interactions between cohesive sediment tracers and natural mud, J. Soils Sediment. 10 (7) (2010) 1401–1414.
[34] R. Whitehouse, A. Manning, Mixing It: How Marine Mud and Sand Interact, Innovation & Research Focus, Institution of Civil Engineering, London, Thomas Telford Services Ltd, 71(2), 2007.
[35] R. Whitehouse, R. Soulsby, W. Roberts, H. Mitchener. Dynamics of Estuarine Muds: A Manual for Practical Applications, Thomas Telford, 2020.
[36] A. Shakeel, Z. Safar, M. Ibanez, L. van Passen, C. Chassagne, Flocculation of clay suspensions by anionic and cationic polyelectrolytes: a systematic analysis, J. Soils Sediment. 20 (2020) 2553–2562.
[37] A.J. Manning, K.R. Dyer, A laboratory examination of floc characteristics with regard to turbulent shearing, Mar. Geol. 160 (1) (1999) 147–170.
[38] A. Shakeel, A. Kirichek, C. Chassagne, Effect of pre-shearing on the steady and dynamic rheological properties of mud sediments, Mar. Pet. Geol. 116 (2020), 104338.
[39] A. Shakeel, P.J.M. van Kan, C. Chassagne, Design of a parallel plate shearing device for visualization of concentrated suspensions, Measurement 145 (2019) 391–399.
[40] H.A. Barnes, A review of the slip (wall depletion) of polymer solutions, emulsions and particle suspensions in viscometers: its cause, character, and cure, J. Non-Newton. Fluid Mech. 56 (3) (1995) 221–251.
[41] A. Shakeel, A. Kirichek, A. Talmon, C. Chassagne, Rheological analysis and rheological modelling of mud sediments: what is the best protocol for maintenance

of ports and waterways? Estuarine, Coastal and Shelf Science (2021) https://doi.org/10.1016/j.ecss.2021.107407. In press.
[42] C. Mobuchon, P.J. Carreau, M.-C. Heuzey, Effect of flow history on the structure of a non-polar polymer/clay nanocomposite model system, Rheol. Acta 46 (8) (2007) 1045–1056.
[43] C. Mobuchon, P.J. Carreau, M.-C. Heuzey, Structural analysis of non-aqueous layered silicate suspensions subjected to shear flow, J. Rheol. 53 (5) (2009) 1025–1048.
[44] L. Ye, A.J. Manning, T.-J. Hsu, Oil-mineral flocculation and settling velocity in saline water, Water Res. 173 (2020), 115569.
[45] M.R. MacIver, Development and usability assessment of a connected resistance exercise band application for strength-monitoring, World Acad. Sci. Eng. Technol. 13 (2019) 340–348, https://doi.org/10.5281/zenodo.
[46] P. Meakin, Fractal aggregates, Adv. Colloid Interface Sci. 28 (1987) 249–331.
[47] F. Maggi, A.J. Manning, J.C. Winterwerp, Image separation and geometric characterisation of mud flocs, J. Hydrol. 326 (1) (2006) 325–348.
[48] A. Shakeel, A. Kirichek, C. Chassagne, Rheological analysis of natural and diluted mud suspensions, J. Non-Newton. Fluid Mech. 286 (2020), 104434.
[49] F.R. Lupi, A. Shakeel, V. Greco, C. Oliviero Rossi, N. Baldino, D. Gabriele, A rheological and microstructural characterisation of bigels for cosmetic and pharmaceutical uses, Mater. Sci. Eng. C 69 (2016) 358–365.
[50] T. Ilstad, A. Elverhøi, D. Issler, J.G. Marr, Subaqueous debris flow behaviour and its dependence on the sand/clay ratio: a laboratory study using particle tracking, Mar. Geol. 213 (1) (2004) 415–438.
[51] Z. Shao, A.S. Negi, C.O. Osuji, Role of interparticle attraction in the yielding response of microgel suspensions, Soft Matter 9 (22) (2013) 5492–5500.
[52] K.N. Pham, G. Petekidis, D. Vlassopoulos, S.U. Egelhaaf, W.C.K. Poon, P.N. Pusey, Yielding behavior of repulsion- and attraction-dominated colloidal glasses, J. Rheol. 52 (2) (2008) 649–676.
[53] A. Ahuja, C. Gamonpilas, Dual yielding in capillary suspensions, Rheol. Acta 56 (10) (2017) 801–810.
[54] A. Potanin, Rheology of silica dispersions stabilized by polymers, Colloids Surf. A Physicochem. Eng. Asp. 562 (2019) 54–60.
[55] A. Shukla, S. Arnipally, M. Dagaonkar, Y.M. Joshi, Two-step yielding in surfactant suspension pastes, Rheol. Acta 54 (5) (2015) 353–364.
[56] J.P. Segovia-Gutiérrez, C.L.A. Berli, J.d. Vicente, Nonlinear viscoelasticity and two-step yielding in magnetorheology: a colloidal gel approach to understand the effect of particle concentration, J. Rheol. 56 (6) (2012) 1429–1448.
[57] A. Nosrati, J. Addai-Mensah, W. Skinner, Rheology of aging aqueous muscovite clay dispersions, Chem. Eng. Sci. 66 (2) (2011) 119–127.
[58] I. Arief, P.K. Mukhopadhyay, Magnetorheology in CoNi nanoplatelet-based MRFs: effect of platelet orientation and oscillatory shear, J. Magn. Magn. Mater. 479 (2019) 326–331.
[59] Z. Varga, V. Grenard, S. Pecorario, N. Taberlet, V. Dolique, S. Manneville, T. Divoux, G.H. McKinley, J.W. Swan, Hydrodynamics control shear-induced pattern formation in attractive suspensions, Proc. Natl. Acad. Sci. 116 (25) (2019) 12193–12198.
[60] M. Das, L. Chambon, Z. Varga, M. Vamvakaki, J.W. Swan, G. Petekidis, Shear driven vorticity aligned flocs in a suspension of attractive rigid rods, Soft Matter 17 (2021) 1232–1245.
[61] C.P. Chu, D.J. Lee, X.F. Peng, Structure of conditioned sludge flocs, Water Res. 38 (8) (2004) 2125–2134.
[62] I.G. Droppo, K. Exall, K. Stafford, Effects of chemical amendments on aquatic floc structure, settling and strength, Water Res. 42 (1–2) (2008) 169–179.
[63] P. Jarvis, B. Jefferson, S.A. Parsons, Floc structural characteristics using conventional coagulation for a high doc, low alkalinity surface water source, Water Res. 40 (14) (2006) 2727–2737.
[64] F. Mietta, C. Chassagne, A.J. Manning, J.C. Winterwerp, Influence of shear rate, organic matter content, pH and salinity on mud flocculation, Ocean Dyn. 59 (5) (2009) 751–763.
[65] H. Fan, X. Liu, H. Wang, Y. Han, L. Qi, H. Wang, Oxygen transfer dynamics and activated sludge floc structure under different sludge retention times at low dissolved oxygen concentrations, Chemosphere 169 (2017) 586–595.
[66] J. Wei, B. Gao, Q. Yue, Y. Wang, W. Li, X. Zhu, Comparison of coagulation behavior and floc structure characteristic of different polyferric-cationic polymer dual-coagulants in humic acid solution, Water Res. 43 (3) (2009) 724–732.
[67] N.B. Wyatt, T.J. O'Hern, B. Shelden, L.G. Hughes, L.A. Mondy, Size and structure of Chlorella zofingiensis/FeCl3 flocs in a shear flow, Biotechnol. Bioeng. 110 (12) (2013) 3156–3163.
[68] W. Xu, B. Gao, R. Mao, Q. Yue, Influence of floc size and structure on membrane fouling in coagulation–ultrafiltration hybrid process—the role of Al13 species, J. Hazard. Mater. 193 (2011) 249–256.
[69] Y.Q. Zhao, Settling behaviour of polymer flocculated water-treatment sludge II: effects of floc structure and floc packing, Sep. Purif. Technol. 35 (3) (2004) 175–183.
[70] H. Zheng, G. Zhu, S. Jiang, T. Tshukudu, X. Xiang, P. Zhang, Q. He, Investigations of coagulation–flocculation process by performance optimization, model prediction and fractal structure of flocs, Desalination 269 (1) (2011) 148–156.
[71] S. Al Ani, K.R. Dyer, D.A. Huntley, Measurement of the influence of salinity on floc density and strength, Geo-Mar. Lett. 11 (3–4) (1991) 154–158.
[72] C. Chassagne, Z. Safar, Modelling flocculation: towards an integration in large-scale sediment transport models, Mar. Geol. 430 (2020), 106361.
[73] K.R. Dyer, A.J. Manning, Observation of the size, settling velocity and effective density of flocs, and their fractal dimensions, J. Sea Res. 41 (1) (1999) 87–95.
[74] D.J. Lee, G.W. Chen, Y.C. Liao, C.C. Hsieh, On the free-settling test for estimating activated sludge floc density, Water Res. 30 (3) (1996) 541–550.
[75] O.A. Mikkelsen, P.S. Hill, T.G. Milligan, Seasonal and spatial variation of floc size, settling velocity, and density on the inner Adriatic Shelf (Italy), Cont. Shelf Res. 27 (3–4) (2007) 417–430.